Net exchanges of methane and carbon dioxide on the Qinghai-Tibetan Plateau from 1979 to 2100

2015 Environ. Res. Lett. 10 085007

(http://iopscience.iop.org/1748-9326/10/8/085007)

Environmental Research Letters

OPEN ACCESS

RECEIVED
10 April 2015

REVISED
18 June 2015

ACCEPTED FOR PUBLICATION
20 July 2015

PUBLISHED
18 August 2015

PAPER

Net exchanges of methane and carbon dioxide on the Qinghai-Tibetan Plateau from 1979 to 2100

Zhenong Jin[1], **Qianlai Zhuang**[1,2], **Jin-Sheng He**[3,4], **Xudong Zhu**[1] **and Weimin Song**[3]

[1] Department of Earth, Atmospheric, and Planetary Sciences, Purdue University, West Lafayette, Indiana 47907, USA
[2] Department of Agronomy, Purdue University, West Lafayette, Indiana 47907, USA
[3] Department of Ecology, College of Urban and Environmental Sciences, Peking University, Beijing 100871, People's Republic of China
[4] Key Laboratory of Adaptation and Evolution of Plateau Biota, Northwest Institute of Plateau Biology, Chinese Academy of Sciences, Xining 810008, People's Republic of China

E-mail: qzhuang@purdue.edu

Keywords: methane, carbon dioxide, climate change, terrestrial ecosystem model, Tibetan Plateau

Supplementary material for this article is available online

Abstract

Methane (CH_4) is a potent greenhouse gas (GHG) that affects the global climate system. Knowledge about land–atmospheric CH_4 exchanges on the Qinghai-Tibetan Plateau (QTP) is insufficient. Using a coupled biogeochemistry model, this study analyzes the net exchanges of CH_4 and CO_2 over the QTP for the period of 1979–2100. Our simulations show that the region currently acts as a net CH_4 source with 0.95 Tg CH_4 y^{-1} emissions and 0.19 Tg CH_4 y^{-1} soil uptake, and a photosynthesis C sink of 14.1 Tg C y^{-1}. By accounting for the net CH_4 emission and the net CO_2 sequestration since 1979, the region was found to be initially a warming source until the 2010s with a positive instantaneous radiative forcing peak in the 1990s. In response to future climate change projected by multiple global climate models (GCMs) under four representative concentration pathway (RCP) scenarios, the regional source of CH_4 to the atmosphere will increase by 15–77% at the end of this century. Net ecosystem production (NEP) will continually increase from the near neutral state to around 40 Tg C y^{-1} under all RCPs except RCP8.5. Spatially, CH_4 emission or uptake will be noticeably enhanced under all RCPs over most of the QTP, while statistically significant NEP changes over a large-scale will only appear under RCP4.5 and RCP4.6 scenarios. The cumulative GHG fluxes since 1979 will exert a slight warming effect on the climate system until the 2030s, and will switch to a cooling effect thereafter. Overall, the total radiative forcing at the end of the 21st century is 0.25–0.35 W m^{-2}, depending on the RCP scenario. Our study highlights the importance of accounting for both CH_4 and CO_2 in quantifying the regional GHG budget.

1. Introduction

Methane (CH_4), second only to carbon dioxide (CO_2), is an important greenhouse gas (GHG) that is responsible for about 20% of the global warming induced by human activity since preindustrial times (IPCC, 2013). Because CH_4 has a much higher global warming potential (GWP) than CO_2 in a time horizon of 100 years, and actively interacts with aerosols and ozone (Shindell *et al* 2009), even small changes in atmospheric CH_4 concentration will have profound impacts on the future climate (Bridgham *et al* 2013, Zhuang *et al* 2013). Quantifying regional and global methane budgets has therefore become a research priority in recent years (Kirschke *et al* 2013). Among all natural sources of CH_4, global wetlands are the single largest source that is responsible for emissions of 142–284 Tg CH_4 per year (Kirschke *et al* 2013, Wania *et al* 2013). CH_4 emissions from wetlands are the net results of CH_4 production under anaerobic conditions, and oxidation by oxygen and transport through the soil and water profile (Olefeldt *et al* 2013). Over 90% of the CH_4 emitted to the atmosphere is oxidized by chemical reactions in the troposphere (Kirschke *et al* 2013), while soil sinks through methanotrophy are indispensable as well (Spahni *et al* 2011, Zhuang *et al* 2013). The relative strength of sources and sinks

determines the global net CH_4 emission on various spatial or temporal scales.

CH_4 emissions from natural wetlands on the Qinghai-Tibetan Plateau (QTP) have drawn increasing attention (Chen *et al* 2013). This world's highest plateau has been a large reservoir of soil carbon for the past thousands of years because of the slow soil decomposition rate and relatively favorable photosynthetic conditions compared with high-latitude cold ecosystems (Kato *et al* 2013). The high carbon storage is distributed over a sporadic landscape that accommodates more than half of China's natural wetlands, and hence the QTP is responsible for 63.5% of CH_4 emissions from natural wetlands in China (Chen *et al* 2013). In recent decades, natural wetlands on the QTP have been expanding (Niu *et al* 2012). With more available soil carbon substrate due to higher plant production and litter fall input (Zhuang *et al* 2010, Piao *et al* 2012), CH_4 emissions from this region have been accelerating and are projected to increase under future climate conditions (Chen *et al* 2013).

Recently, several site-level studies have advanced our understanding of CH_4 emissions from wetlands on the QTP. Major emissions occur during the growing season, and net effluxes can vary from −0.81 to 90 $\mu g\ m^{-2}\ h^{-1}$ at different locations (Jin *et al* 1999, Hirota *et al* 2004, Kato *et al* 2011, Chen *et al* 2013). Furthermore, flux tower observations indicate that non-growing season CH_4 emissions in an alpine wetland can contribute to around 45% of the annual emissions (Song *et al* 2015). These high variations in space and time are the results of complex environmental control over CH_4 emissions. Chen *et al* (2009) found that water table depth is a key factor that controls the spatial variations in CH_4 emissions in an open fen on the eastern edge of the QTP. Soil temperature is also an important regulator of CH_4 emissions, since the QTP is underlain by extensive permafrost (Chen *et al* 2010, Yu *et al* 2013). In addition, plant succession from cyperaceous to gramineous species during wetland degradation will result in a net reduction in plant-aided transport of CH_4 to the atmosphere (Hirota *et al* 2004, Chen *et al* 2010). In contrast to the noticeable progress in field measurements and experiments, there is still a lack of systematic and quantitative understanding of the regional CH_4 budget for the QTP. The estimated wetland CH_4 emissions of 0.56–2.47 Tg per year (Jin *et al* 1999, Ding and Cai 2007, Chen *et al* 2013, Zhang and Jiang 2014) should be viewed as preliminary results, because they are calculated using a book-keeping approach, i.e. the estimate is a product of the wetlands area, the flux measurements at a few sites, and the approximate number of frozen-free days. In addition, the role of the soil consumption of atmospheric CH_4 in most of the alpine steppe and meadow zones is highly uncertain (Kato *et al* 2011, Wei *et al* 2012, Zhuang *et al* 2013), but should not be neglected when quantifying the regional net methane exchange (NME). More importantly, it is necessary to consider both CH_4 and CO_2 dynamics in quantifying the regional GHG budget of the QTP.

Here, we quantify the GHG budget of CH_4 and CO_2 for both historical data and for the 21st century on the QTP using a coupled biogeochemistry model, the terrestrial ecosystem model (TEM) (Zhuang *et al* 2004, Zhu *et al* 2013). The model is calibrated against field observations using a global optimization method and applied for the period 1979–2100. The carbon-based GHG effect of CH_4 and CO_2, represented by the NME and net ecosystem production (NEP, calculated as the difference between the gross primary production and ecosystem respiration), are examined using radiative forcing impact (Frolking *et al* 2006). Our research objectives are to: (i) quantify sources and sinks with respect to CH_4 and CO_2 in the historical period of 1979–2011; (ii) explore how the NME and NEP will respond to future climate changes; (iii) attribute the relative contribution of CH_4 and CO_2 to the regional carbon budget and radiative forcing, and (iv) identify research priorities to reduce quantification uncertainties of the GHG budget in the region.

2. Methods

2.1. Model framework

The TEM is a process-based ecosystem model that simulates the biogeochemical cycles of C and N between terrestrial ecosystems and the atmosphere (Zhuang *et al* 2004, 2010). Within the TEM, two submodels, namely the soil thermal model (STM) and the updated hydrological model (HM), are designed to simulate the soil thermal profile and hydrological processes with a daily time step, respectively. The STM is well documented for arctic regions and the Tibetan Plateau (e.g. Zhuang *et al* 2010, Jin *et al* 2013). The HM, inherited from the water balance model (WBM) (Vörösmarty *et al* 1989), has six layers for upland soils and a single box for wetland soils (Zhuang *et al* 2004). We assume the maximum wetland water table depth to be 30 cm following Zhuang *et al* (2004), so that soils are always saturated below 30 cm. These physical variables then drive the carbon/nitrogen dynamics module (CNDM), which uses spatially explicit information on climate, elevation, soil, vegetation and water availability, as well as soil- and vegetation-specific parameters, to estimate the carbon and nitrogen fluxes and pool sizes of terrestrial ecosystems (Zhuang *et al* 2004, 2010).

The methane dynamics module (MDM) was first coupled with the TEM by Zhuang *et al* (2004), to explicitly simulate the processes of CH_4 production (methanogenesis), CH_4 oxidation (methanotrophy) and CH_4 transport between the soil and the atmosphere. During the simulation, the water table depth estimated by the HM, the soil temperature profile estimated by the STM and the labile soil organic carbon

estimated by the CNDM, as well as other soil and meteorological information, were fed into the MDM so that the whole TEM and MDM are fully coupled (figure S1). CH_4 production, a strictly anaerobic process, is modeled as a function of the labile carbon substrate, temperature, pH, and the redox potential in saturated soils. CH_4 oxidation, occurring in the unsaturated zone, depends on the soil CH_4 and O_2 concentration, temperature, moisture and the redox potential. The net CH_4 fluxes at the soil/water–atmosphere boundary are summations of different transport pathways (i.e. diffusion, ebullition and plant-aided emission), with a positive value indicating a CH_4 source to the atmosphere and a negative value for a CH_4 sink (Zhuang *et al* 2004).

2.2. Field measurements and model calibration

Data used to calibrate the TEM were measured at the Luanhaizi wetland on the northeastern Tibetan Plateau (37° 35′ N, 101° 20′ E) from July 2011 to December 2013. This wetland is classified as an alpine Marsh, and has accumulated rich soil carbon of 24.5% on average for the top 30 cm soil layer due to slow decomposition. An eddy covariance measurement system was installed at a height of 2 m above the wetland surface, which recorded CH_4 fluxes every half hour (Yu *et al* 2013). A micro-meteorology station was set up adjacent to the eddy covariance tower to measure major environmental variables at half hour frequency, including air and soil temperature, total precipitation, downward shortwave irradiance and relative humidity. We parameterized the STM using the measured soil temperature at a 5 cm depth. Major parameters for the MDM were calibrated so that the simulations match the observed CH_4 fluxes. Due to a lack of high quality measurements, the water table depth was calibrated indirectly by fitting the final CH_4 fluxes, and compared to the observed precipitation as a reference. Parameters for the CNDM were obtained from our previous modeling studies on the Tibetan Plateau (Zhuang *et al* 2010, Jin *et al* 2015).

The mathematical structure of the TEM is fixed and can be expressed as below:

$$\hat{Y} = f(X|\theta) + e \tag{1}$$

where f is a conceptual function that represents all processes within the TEM, $\hat{Y} = (y_1, y_2, \ldots y_N)$ is a vector of the model outputs (e.g. time series of daily soil temperature or CH_4 fluxes), X is the model input data, $\theta = (\theta_1, \theta_2, \theta_3, \ldots, \theta_n)$ are n unknown parameters to be calibrated, and $e = \{e(\theta)_1, e(\theta_2), \ldots, e(\theta_N)\}$ are independently and identically distributed (i.i.d.) errors with zero mean and constant variance. The goal of model calibration with classical methods is thus to find a parameter set θ such that the predefined statistics of e can be minimized. In contrast, Bayesian theory treats θ as random variables having a joint posterior probability density function (pdf). The posterior pdf of θ can be evolved from the prior distribution with observations Y such that:

$$p_{\text{post}}(\theta|Y) = \frac{L(Y|\theta)p_{\text{prior}}(\theta)}{\int L(Y|\theta)p_{\text{prior}}(\theta)} \tag{2}$$

where $L(Y|\theta)$ is the likelihood function. Assuming a non-informative prior in the form of $p(\theta) \propto \sigma^{-1}$ and residuals which are i.i.d normal (Vrugt *et al* 2003), the likelihood of a specific parameter set θ' can be computed as:

$$L(\theta'|Y) = \exp\left[-\frac{1}{2}\sum_{i=1}^{N}\left(\frac{e(\theta')_i}{\sigma}\right)^2\right] \tag{3}$$

The influence of σ can be integrated out when $L(\theta'|Y)$ is plugged into equation (2), so that the posterior pdf of θ' is:

$$p_{\text{post}}(\theta'|Y) \propto \left[\sum_{i=1}^{N} e(\theta')_i{}^2\right]^{-0.5\times N} \tag{4}$$

For complex nonlinear system models like the TEM, however, it is impossible to obtain an explicit expression for $p_{\text{post}}(\theta'|Y)$, making analytical optimization out of the question (Vrugt *et al* 2003). Alternatively, Markov chain Monte Carlo (MCMC) methods are well suited to solving these problems.

In this study, we implemented an adaptive MCMC sampler, named the shuffled complex evolution Metropolis algorithm (SCEM-UA) for global optimization and parameter uncertainty assessment. While the theoretical bases and computational implementation of the SCEM-UA can be found in (Vrugt *et al* 2003), we outline the key steps with an example of STM optimization below:

(i) Initialize parameter space. Select parameters to be calibrated, and assign prior range to each parameter (table 1).

(ii) Generate sample. Randomly sample s sets of parameter combination $\{\vec{\theta_1}, \vec{\theta_2}, \ldots, \vec{\theta_s}\}$ from the uniform prior distribution, where $\vec{\theta_i}$ is a vector of eight parameters for the STM in table 1.

(iii) Rank sample points. Compute the posterior density of each $\vec{\theta_i}$ using equation (3), and sort the s points in 8-dimensions with decreasing order of posterior density. Store the s points and their corresponding posterior in array D with dimensions of $s \times 9$.

(iv) Initialize Markov chains. Assign the first k elements of D as the starting locations of k sequences.

(v) Partition D into complexes. Partition s rows of D into k complexes $\{C^1, C^2, \ldots C^k\}$, such that each complex contain $m = s/k$ points. More specifically, the $i-$th complex is assigned every $k(j-1)+i$ rows of D, where $j = 1, \ldots, m$.

Table 1. Prior and posterior range of parameters calibrated in Soil Thermal Module (STM) and Methane Dynamics Module (MDM).

Acronym	Definition	Prior	Posterior[a]	Unit
	Soil Thermal Model			
condt1	Thawing soil thermal conductivity for first layer	[0.6, 3.5]	[2.724, 3.266]	$W\,m^{-1}\,K^{-1}$
condf1	Frozen soil thermal conductivity for first layer	[0.6, 4.0]	[0.6, 0.874]	$W\,m^{-1}\,K^{-1}$
condt2	Thawing soil thermal conductivity for second layer	[0.6, 3.5]	[1.194, 2.110]	$W\,m^{-1}\,K^{-1}$
condf2	Frozen soil thermal conductivity for second layer	[0.6, 4.0]	[0.723, 1.236]	$W\,m^{-1}\,K^{-1}$
spht1	Thawing soil heat capacity for first layer	[0.5, 4.0]	[1.604, 2.615]	$MJ\,m^{-3}\,K^{-1}$
sphf1	Frozen soil heat capacity for first layer	[0.5, 4.0]	[2.066, 3.018]	$MJ\,m^{-3}\,K^{-1}$
spht2	Thawing soil heat capacity for second layer	[0.5, 4.0]	[1.474, 2.445]]	$MJ\,m^{-3}\,K^{-1}$
sphf2	Frozen soil heat capacity for second layer	[0.5, 4.0]	[1.655, 2.586]	$MJ\,m^{-3}\,K^{-1}$
	Methane Model			
MGO	Maximum potential CH_4 production rate	[0.2, 0.7]	[0.377, 0.545]	$\mu mol\,L^{-1}\,h^{-1}$
PQ10	Dependency of CH_4 production on soil temperature	[2.0, 3.5]	[2.179, 2.654]	unitless
MaxFresh	Maximum daily NPP for a particular ecosystem	[2.0, 8.0]	[5.606, 7.164]	$gC\,m^{-2}\,day^{-1}$
PROREF	Reference temperature in Q10 function	[−3.0, 1.0]	[−1.546, −0.256]	°C
winflxR	Winter CH_4 emission ratio	[0.4, 0.9]	[0.628, 0.756]	Unitless
Qdmax	Maximum drainage rate below water table	[0.1, 2.0]	[0.251, 0.447]	$Mm\,d^{-1}$

[a] Posterior range is defined as the shortest interval that include 68% of the total samples.

(vi) Evolve each complex and sequence. Use the sequence evolution Metropolis algorithm to evolve each sequence and complex (Vrugt *et al* 2003).

(vii) Shuffle complexes. Combine each point in all complexes back with D in order of decreasing posterior density.

(viii) Apply stop rule. Stop when convergence criteria are satisfied; otherwise, go to step (v). A maximum of 100 000 runs for the STM and 200 000 runs for the MDM was imposed to override the stopping rule for computational considerations.

We selected $s = 500$ and $k = 10$ following Vrugt *et al* (2003) for complex model optimization. Given the complexity of our coupled-TEM, each run cost at least 1 minute, including reaching model equilibrium, model spin-up and transient simulations for the period 2011–2013. In this case, parallel implementation of the SCEM-UA was required to obtain computational efficiency. We developed a parallel R version of the SCEM-UA using the Open Message Passing Interface (MPI; Gabriel *et al* 2004) and the Rmpi package (Yu *et al* 2002) on Purdue University's Conte computer clusters. This parallel SCEM-UA program would evoke a master node that controlled the workflow and message communication among 10 slave nodes. Each slave node was responsible for the computation of posterior density (i.e. step (iii)) and for the evolution of a specific group of complexes and sequences (i.e. step (vi)). Compared to the parallel implementation of the SCEM-UA in Vrugt *et al* (2006), our program does not require the target model (e.g. the TEM in this study) to be written in the MPI structure, but only treats it as a black box to be executed using a system call in R. The source code for this parallel R version of the SCEM-UA is available upon request.

2.3. Regional extrapolation

To make spatiotemporal estimates of the CO_2 and CH_4 fluxes on the QTP using the TEM, the model was run at a spatial resolution of 8×8 km and with a daily time step from 1979 to 2100. Static data including vegetation types, elevation, and soil texture were the same as those in Jin *et al* (2013). Soil pH data was derived from the China Dataset of Soil Properties for Land Surface Modeling by Wei *et al* (2013). The wet soil extent from Papa *et al* (2010) was used to determine the distribution of wetlands (CH_4 source) and uplands (CH_4 sink) within each pixel (figure 1(b)). For this temporally dynamical and 25×25 km resolution data set, we interpolated the maximum fractional inundation over 8×8 km using the nearest neighbor approach. It should be noted that the actual wetland distribution was less continuous than was shown in figure 1(b). The inland water body was excluded based on the IGBP DISCover Database (Loveland *et al* 2000). Seasonal flooding of the wetland was indirectly represented by the fluctuation of the water table depth below and above the soil surface in our model. Climate input data for the historical period of 1979–2011, including radiation, precipitation, air temperature and vapor pressure, were interpolated from the latest global meteorological reanalysis product ERA-interim (0.75° grid) published by the European

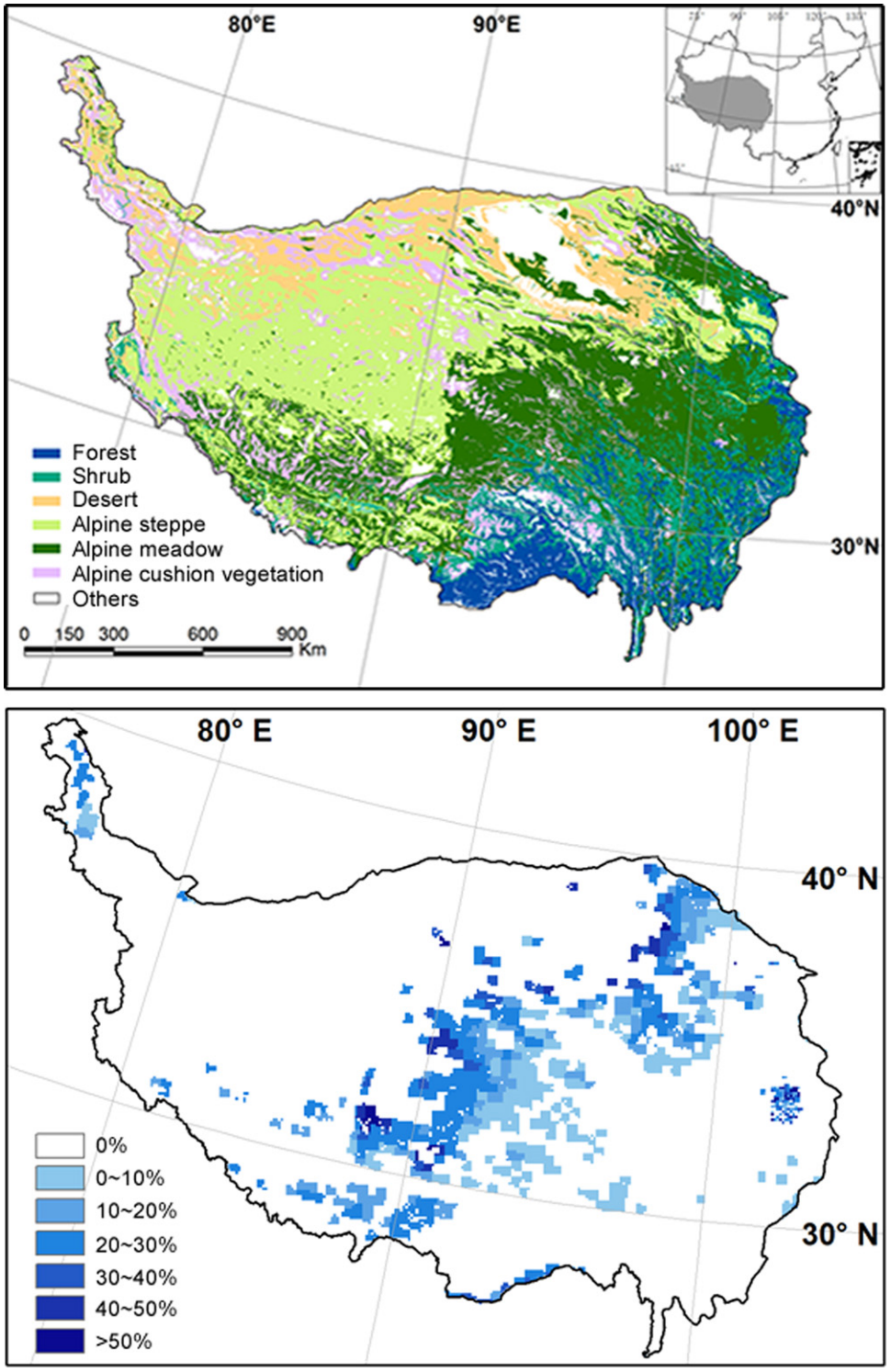

Figure 1. Vegetation distribution of Qinghai-Tibetan Plateau (upper panel) and maximum fractional inundation (lower panel).

Centre for Medium-Range Weather Forecasts (ECMWF) (Dee *et al* 2011). To reduce bias in air temperature caused by complex topography, we used elevation as a covariate during interpolation according to Frauenfeld *et al* (2005). Future climate scenarios from 2006 to 2100 were generated under four representative concentration pathways (RCPs) with six global climate models (GCMs) within Coupled Model Inter-comparison Project phase 5 (CMIP5), including: CESM1-CAM5, GFDL-CM3, GISS-E2-H, HadGEM2-ES, MPI-ESM-Mr and MRI-CGCM3 (figures S3, S4). A total of 24 simulations (4 scenarios × 6 GCM datasets) were processed to construct future projections. These selected GCMs, compared with many other candidates, in general had smaller biases in surface temperature and total precipitation across the Tibetan Plateau (Su *et al* 2013). A detailed description of these CMIP5 GCMs and the data processing method are provided in methods S1.

2.4. Analysis

To highlight the spatial pattern of the climate induced changes in GHG fluxes, we calculated the spatial difference between baseline simulations using ECMWF data in the 2000s and future predictions with four RCP scenarios in the 2090s. A statistical test of the difference in means was performed, and regions with statistical insignificance ($\alpha = 0.05$) were masked out. To quantify the GHG effect of the continuous CH_4 and CO_2 fluxes from the QTP for the study period of 1979–2010, we calculated the net radiative forcing impact according to Frolking *et al* (2006). The lifetime of an individual net input of CH_4 into the background atmosphere was represented by a first-order decay function such that:

$$rCH_4(t) = r_0 \times \exp\left(-t/\tau_{CH4}\right) \quad (5)$$

where r_0 is the initial CH_4 perturbation, and τ_{CH4} is the adjusted time for CH_4 (~12 y). A linear superposition of 5 different first-order decay pools was used to describe the more complicated behavior of CO_2 in the atmosphere:

$$rCO_2(t) \sim \sum_{i=0}^{4} f_i \exp\left(-t/\tau_i\right) \quad (6)$$

where the fraction of each pool, f_i, and the pool specific adjustment time, τ_i, were set to be 26%, 24%, 19%, 14%, 18% and 3.4, 21, 71, 421, 10^8 y, respectively (Frolking *et al* 2006). The instantaneous total radiative forcing from individual gas contributions since the reference time (here the year 1979) is given by:

$$\mathrm{RF}(t) = \sum_{i=0}^{5}\left(\xi_i A_i f_i \cdot \int_o^t \Phi_i(s) \exp\left(-(t-s)/\tau_i\right)\mathrm{d}s\right) \quad (7)$$

in which $i = 0$–4 is CO_2 and $i = 5$ is CH_4, and ξ_i is a multiplier for indirect effects (1.3 for CH_4 and 1.0 for CO_2), A_i is the GHG radiative efficiency (1.3×10^{-13} W m^{-2} kg^{-1} for CH_4 and 0.0198×10^{-13} W m^{-2} kg^{-1} for CO_2), f_i is the fractional multiplier (1 for CH_4 and see equation (6) for CO_2 values), and $\Phi_i(s)$ is the net flux of GHG i at time s relative to the reference year of 1979. The integral term is thus the cumulative flux of gas i at time t since the reference start point (i.e. the year 1979) after partial to complete decay in the atmosphere. The numerical integration was applied with an annual time step. It should be noted, however, that our calculation here was only for the goal of comparing the relative contributions of CO_2 and CH_4 fluxes since 1979 to the radiative forcing, rather than to give an accurate estimation of the absolute values of the GHG effect.

3. Results

3.1. Model optimization and validation

By applying the SCEM-UA method, initial parameter ranges evolved into narrower posterior intervals (table 1). Both the STM and MDM outputs were able to reproduce the seasonal dynamics of the observed daily soil temperature and CH_4 fluxes (figure 2). The adjusted R^2 and RMSE for the soil temperature simulated with the optimal STM are 0.95 and 1.88 °C, respectively. The model performance is comparable with other modeling results (Wania *et al* 2009, Jin *et al* 2013, Zhu *et al* 2014), with only one underestimation during the summer of 2013. The MDM also performed well ($R^2 = 0.82$, RMSE = 18.41 mg CH_4 m^{-2} day^{-1}) in capturing the annual magnitude, cycling and a small peak of CH_4 burst in spring. Considering the uncertainties in the CH_4 flux measurements (Yu *et al* 2013) and the CH_4 model structures (Wania *et al* 2013), our model performance was comparable with similar studies (Wania *et al* 2009, Lu and Zhuang 2012, Zhu *et al* 2014). Parameter uncertainty was well constrained (figures 2(a), (c)), indicating that a global search near the optimal space would produce many parameter sets to allow model simulation matching the observations. The water table depth followed the observed daily precipitation pattern (figure 2(b)). A severe drought was detected for the 2012 summer, which was also reflected by the distinctively low CH_4 emission during that year.

Due to a limited number of available field studies of CH_4 fluxes on the QTP, our model validation was done by comparing values reported in the literature to our simulations for the nearest 8×8 km pixel (table 2). Model estimates reasonably match most field measurements with respect to the mean and range, except for an apparent underestimation of the exceptionally high CH_4 emission rate from the littoral zone in Chen *et al* (2009). Considering the high variation among field measurements from different wetland types and vegetation covers, the model simulations were able to fit the mean ($R^2 = 0.87$, RMSE = 67 for all data and $R^2 = 0.96$, RMSE = 21 mg CH_4 m^{-2} day^{-1} excluding Chen *et al* (2009)). The validation gave us confidence for model extrapolation and regional CH_4 budget estimation.

3.2. Spatiotemporal trends of CO_2 and CH_4 fluxes

Our estimated annual regional mean net primary production (NPP) (145–170 gC m^{-2} y^{-1}) increased slightly for the historical period, and fluctuated under future scenarios (figure 3(a)). NPP increased almost 40% under RCP6.0 (241 ± 22.3 gC m^{-2} y^{-1}) and 50% under RCP8.5 (252 ± 22.4 gC m^{-2} y^{-1}) at the end of the 21st century compared to the 2000s. RCP2.6 and RCP4.5 showed a similar trend in NPP under higher emission scenarios before the 2050s, but leveled off thereafter at around 210 and 230 gC m^{-2} y^{-1}, respectively. Simulated regional mean NEP showed high variation around 0 gC m^{-2} y^{-1} for the period 1979–2011, and decreased continually under future projections except for RCP8.5 (figure 3(b)). The NEP density was lowest under RCP4.5 (−33.1 ± 9.5 gC m^{-2} y^{-1}), followed by RCP6.0 (−30.3 ± 11.4 gC m^{-2}

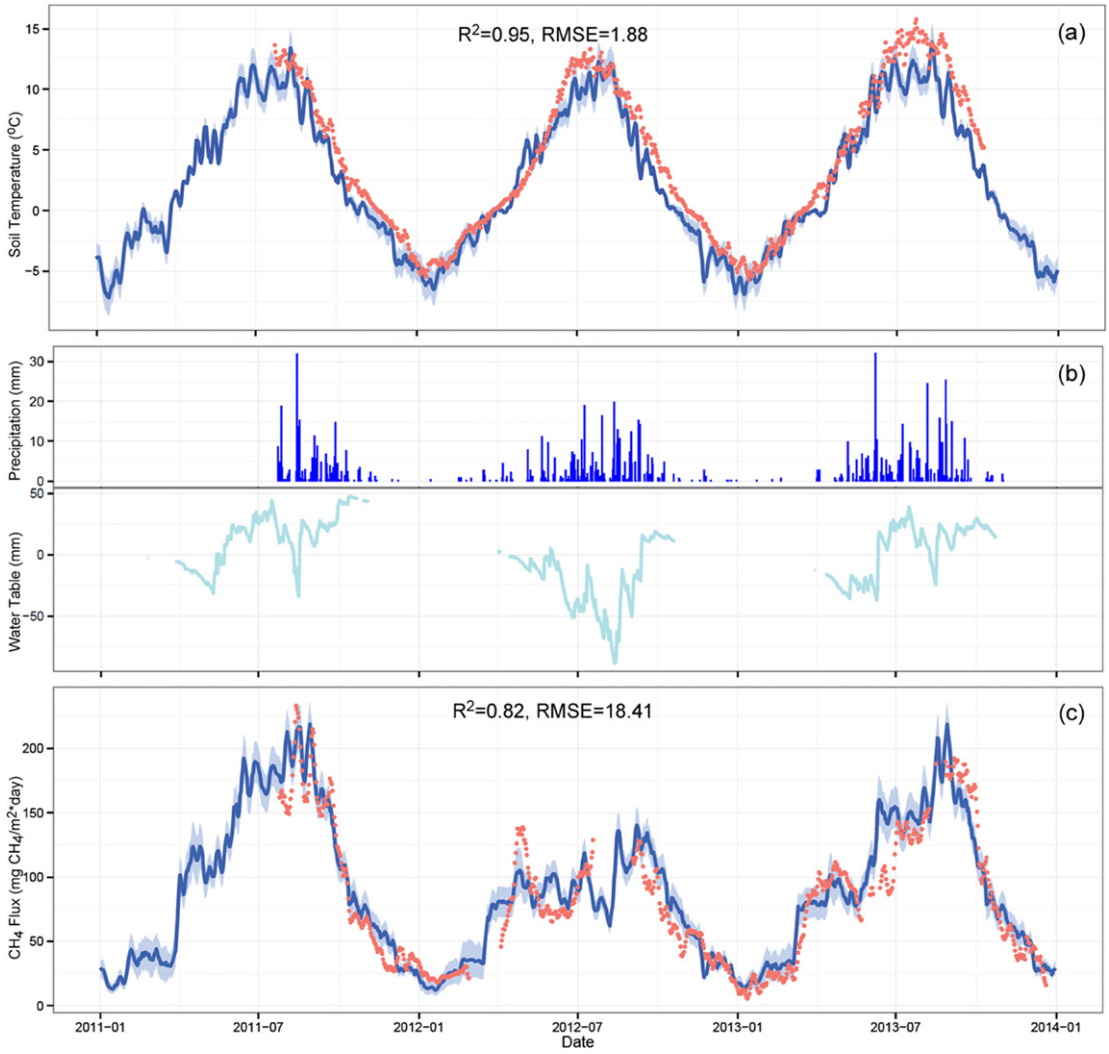

Figure 2. Simulated and observed soil temperatures at 5 cm depth (a), water table depth (b) and CH_4 fluxes (c) at Luanhaizi wetland station. Solid blue lines show the optimal simulation, while shades of light blue are the 95% range of simulations with the top 500 parameter combinations. Red dots are observations. Water table depth is compared with observed daily precipitation data.

y^{-1}) and RCP2.6 (-26.8 ± 11.5 gC m^{-2} y^{-1}) for the 2090s. Under RCP8.5, the NEP density decreased to the 2060s but reversed to -19.5 ± 16.1 gC m^{-2} y^{-1}, possibly because heterogeneous soil respiration (R_H; figure S5) was stimulated more than NPP under this warmest and wettest scenario.

Simulated annual mean CH_4 emissions from potential wetland areas increased gradually from 6.3 gCH_4 m^{-2} y^{-1} in 1979 to 8.5 in the 2050s under different scenarios, but diverged noticeably thereafter (figure 3(c)). The highest emissions for the 2090s from RCP8.5 projections (12.7 ± 1.9 gCH_4 m^{-2} y^{-1}) increased 70% relative to the beginning of the 21st century, followed by 46%, 30% and 16% under RCP6.0, RCP4.5 and RCP2.6, respectively. The relative change percentages of CH_4 emissions were in general higher than those of NPP, implying that CH_4 production was more favored than photosynthesis under future climate conditions. Annual mean CH_4 uptake density (increased from 0.13 in the early 1980s to 0.17 gCH_4 m^{-2} y^{-1} around the 2050s, and ended up between 0.16 to 0.23 gCH_4 m^{-2} y^{-1} in the 2090s) was much smaller than that of emissions, while the inter-annual variations were similar under the four RCP scenarios (figure 3(d)).

Spatial patterns of the decadal mean NME showed substantial variations over the QTP (figure 4). For the 2000s, net CH_4 emissions simulated using reanalysis data were similar to the average of the RCP scenarios (figures 4(a) and (b)), with high net CH_4 emissions occurred at Zoige wetland and in the southwest part of the QTP. Net CH_4 sinks based on the two maps were comparable in magnitude, but high CH_4 uptakes were found at the southern edge of the QTP in figure 4(a) rather than in the northeastern part in figure 4(b). At the end of the 21st century, the NME increased noticeably with respect to the magnitude over the QTP except for some southeastern parts (figures 1(c)–(f)). Among the models, RCP8.5 led to the strongest CH_4 emissions in wetlands and the highest CH_4 consumption in uplands. The difference in means between the RCP scenarios and the 2000s historical mean was

Table 2. Comparison between model simulations and literature reported field measurements of daily CH_4 flux density (mg CH_4 m^{-2} day^{-1}).

			Observation		Simulation		
Location	Measurement time	Vegetation type	Mean	Range	Mean	Range	References
33.93N, 102.87E	Jun.–Sep., 2005-2007	Kobresia tibetica	64.1	n.a.	171.5	[135.5, 208.8]	Chen *et al* 2013
		Cychrus muliensis	311.28	n.a.			
		Eleocharis valleculosa	266.2	n.a.			
33.1N, 102.03E	Jun.–Aug., 2006-2007		362.4	[−2.4, NA]	205.5	[147.2, 264.6]	Chen *et al* 2009
32.78N, 102.53E	May–Oct., 2001-2002	Cychrus mmuliensis	71.04	[3.8, 240]	72.9	[46.7, 96.7]	Ding *et al* 2004
37.48N, 101.2E	Jul.–Sep., 2002	Hydrocotyle vulgaris	214	n.a.	163.9	[136.8, 181.5]	Hirota *et al* 2004
		Carex allivescers	196	n.a.			
		Scirpus distigmaticus	99.5	n.a.			
		Potamogenton pectinatus	33.1	n.a.			
35.65N, 98.8E	Jul. 24–Aug. 8, 1996		43.9	[−4.4, 147.6]	61.8	[50.2, 70.6]	Jin *et al* 1998
	Apr.–Sep., 1997		37.3	[6.5, 71.9]	46.3	[31.3, 66.9]	Jin *et al* 1999

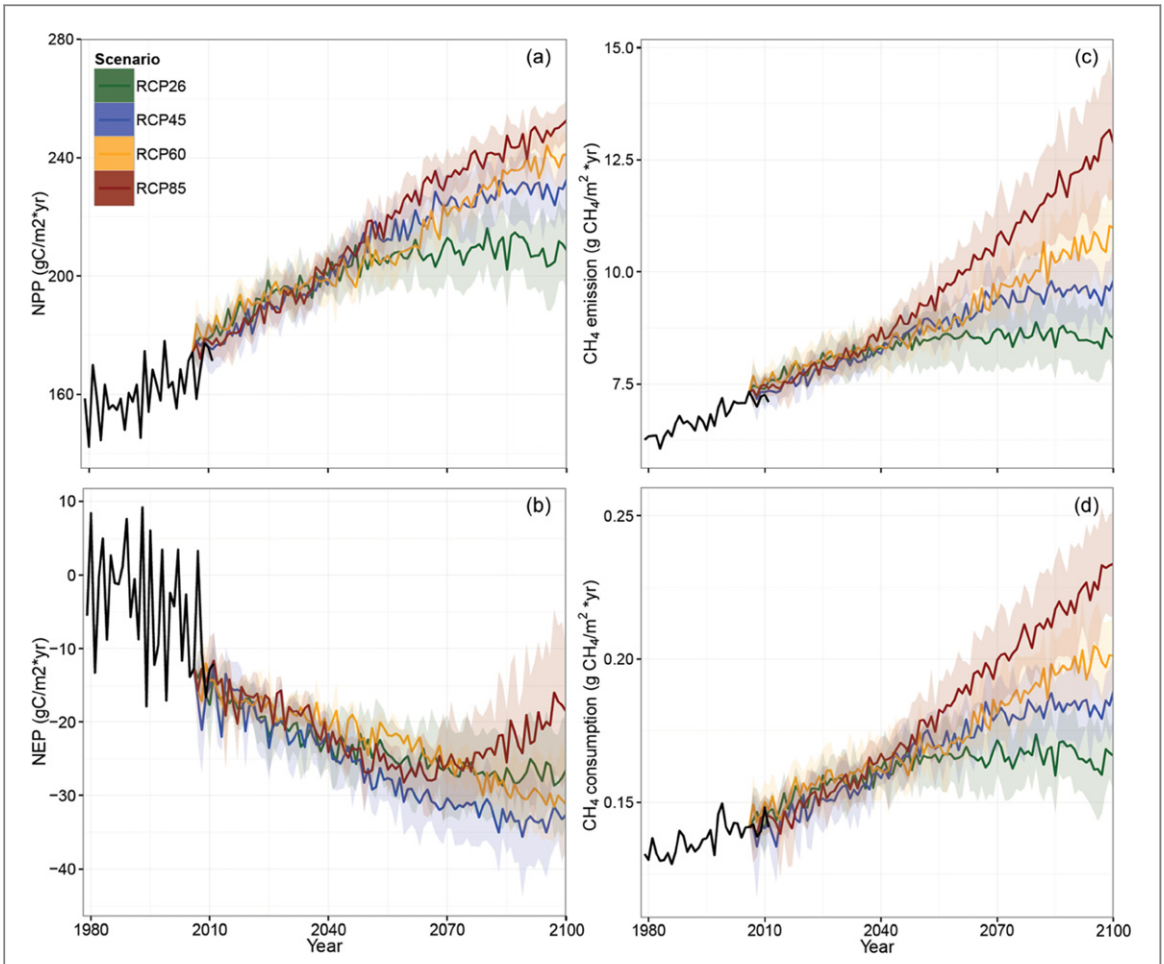

Figure 3. Annual trends of (a) mean net primary production (NPP); (b) mean net ecosystem production (NEP); (c) mean CH_4 emissions from potential wetland areas, and (d) mean CH_4 consumption from upland area for the period 1979–2100. Solid black line represents historical data from 1979 to 2011. Solid color lines are multi-model means under different RCP scenarios; shading represent one standard deviation.

statistically significant ($\alpha = 0.05$) for most of the study area (figures S6(a)–(d)). Future climate change would strengthen the upland CH_4 sink in the inner QTP, and substantially stimulate wetland CH_4 emission in northeastern regions. For simulated NEP, most of the study region had a negative value (i.e. CO_2 sink), with the magnitude up to -30 gC m^{-2} y^{-1} during the 2000s (figures 5(a) and (b)). The patterns were comparable with contemporary estimation for alpine grasslands by Zhuang *et al* (2010) and Piao *et al* (2012). Strong CO_2 sinks occurred in the southeast of the QTP, where forest and shrubs were the dominant vegetation cover (figure 1(a)). CO_2 sources accounted for a very limited portion of the total study area. Spatial patterns of NEP evolved substantially under future scenarios (figures 5(c)–(f)). The QTP became a uniform carbon sink under RCP2.6, indicating disproportional climate impacts on different ecosystem types. Increases in NEP were profound under two median scenarios, with differences statistically significant ($\alpha = 0.05$) for most of the grassland (figures S6(f), (g)). Among these, the highest sink (up to 50 gC m^{-2} y^{-1}) occurred in the forest ecosystem under RCP4.5 and in meadow regions under RCP6.0. NEP under RCP8.5 was distinctively lower than results under other scenarios and not statistically different from the historical 2000s mean (figure S6(h)), suggesting similar changes in the magnitude of NPP and R_H for all ecosystem types.

3.3. Regional GHG budget

Our estimate of the total CH_4 emissions from natural wetland over the QTP was 0.95 Tg CH_4 y^{-1} during the 2000s, which was within the estimation range of 0.13–2.47 Tg CH_4 y^{-1} from several other studies (table 3). The high variation among different estimates was mainly due to the uncertainty in wetland area estimates. Total CH_4 consumption from those upland soils were 0.19 Tg CH_4 y^{-1} (i.e. 20% of the regional CH_4 emissions) for the 2000s, and increased slower than emissions under future scenarios (table 4), indicating that the QTP was likely to be a stronger CH_4 source in the 21st century. The simulated regional NEP of -10.22 Tg C y^{-1} for the period 2006–2011 was lower than those for other modeling studies covering similar regions (Zhuang *et al* 2010, Piao *et al* 2012), but higher than that of Yi *et al* (2014). The near neutral properties of the historical NEP (also see figure 3(b)) were consistent with the results of Fang *et al* (2010),

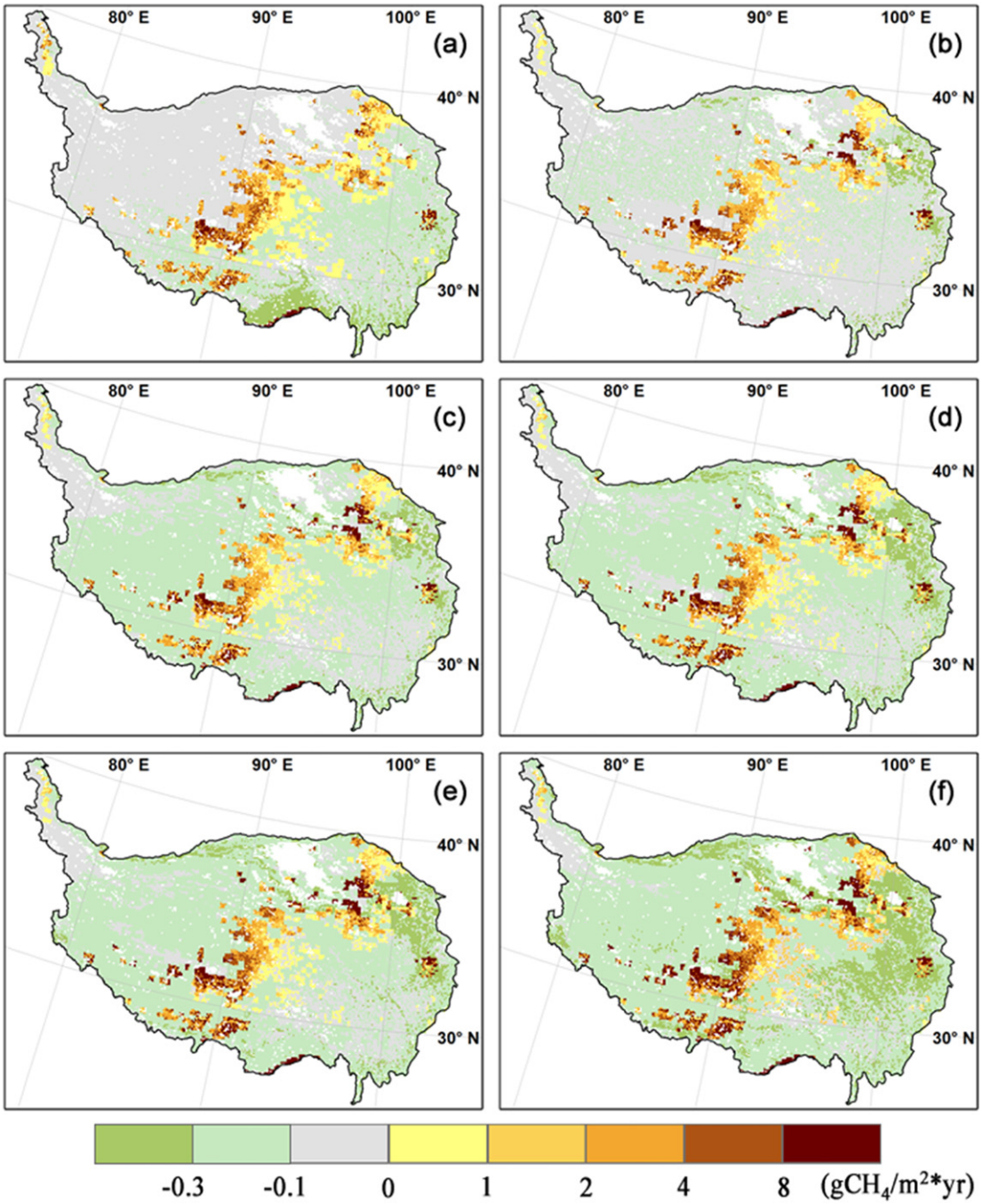

Figure 4. Spatial patterns of mean annual net methane exchange (NME) under different climate scenarios: (a) ECMWF reanalysis data for the 2000s; (b) mean CMIP5 RCPs from 2006–2010; (c) CMIP5 RCP2.6 for the 2090s; (d) CMIP5 RCP4.5 for the 2090s; (e) CMIP5 RCP6.0 for the 2090s; (f) CMIP5 RCP8.5 for the 2090s. Positive values indicate net emissions.

who found that soil C stock in China's grassland did not show a significant change during the past two decades. Future NEP increased under all RCP scenarios (table 4). Counter-intuitively, higher increases in NEP occurred under RCP4.5 and RCP6.0 instead of the warmest and wettest RCP8.5, indicating that carbon accumulation was more likely favored with modest warming and wetting.

Instantaneous radiative forcing due to net CH_4 emission and net CO_2 sequestration since 1979 increased to a plateau during the 1990s, dropped to zero around the 2010 s, and decreased almost linearly afterwards (figure 6(a)). Therefore, climate change in the 21st century is likely to trigger negative feedback (cooling) in the climate system. Among these, the fastest decreased rate occurred under RCP4.5, indicating that this moderate climate warming scenario stimulated vegetation production much more than the methanogenesis process. A seemingly level-off trend after the 2080s was identified for the RCP8.5 scenario, most likely because of declining NEP (figure 3(b)). Cumulative radiative forcing was positive until the 2030s, and become negative in an accelerated manner (figure 6(b)). Thus, the cumulative GHG fluxes from

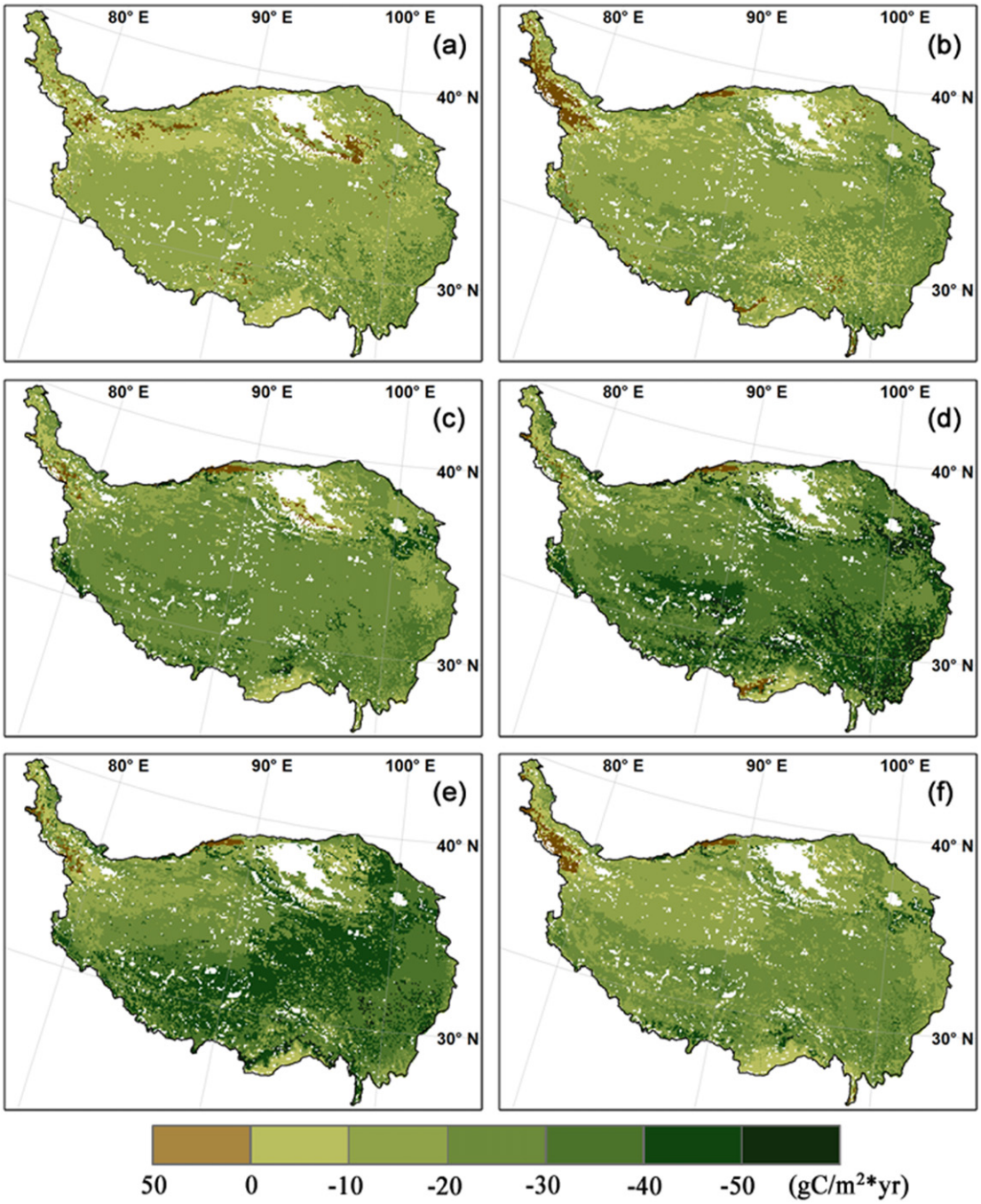

Figure 5. Spatial patterns of mean annual net ecosystem production (NEP) under different climate scenarios: (a) ECMWF reanalysis data for the 2000s; (b) mean CMIP5 RCPs from 2006–2010; (c) CMIP5 RCP2.6 for the 2090s; (d) CMIP5 RCP4.5 for the 2090s; (e) CMIP5 RCP6.0 for the 2090s; (f) CMIP5 RCP8.5 for the 2090s. Negative values indicate carbon sinks.

Table 3. Existing estimates of CH_4 emissions from wetland and alpine plant communities on the Qinghai-Tibetan Plateau.

			Wetland Area	Total	
Methods	Spatial Domain	Period	($\times 10^4$ km^2)	(Tg CH_4 y^{-1})	Source
Inventory	Freshwater wetlands	1996–1997	18.8	0.7–0.9	Jin *et al* 1999
Inventory	Natural wetlands[a]	2001–2002	5.52	0.56	Ding and Cai 2007
Inventory	Alpine meadow	2003–2006	87.5	0.13	Cao *et al* 2008
Meta-Analysis	Natural wetlands			1.49	Chen *et al* 2013
Meta-Analysis	Natural wetlands		3.76	1.04	Zhang and Jiang 2014
TEM	Natural wetlands	1995–2005	11.5	2.47	Xu *et al* 2010
Coupled-TEM	Natural wetlands	2001–2011	13.4	0.95	This study

[a] Natural wetlands include peatlands, freshwater marshes, salt marshes and swamps.

Table 4. Decadal mean of regional greenhouse gas budget.

		2000s	2050s	2090s
CH_4 Emission ($Tg\,CH_4\,y^{-1}$)	ECMWF	0.95		
	RCP2.6	0.99	1.14	1.13
	RCP4.5	0.97	1.18	1.28
	RCP6.0	1.00	1.17	1.42
	RCP8.5	0.99	1.27	1.68
CH_4 Consumption ($Tg\,CH_4\,y^{-1}$)	ECMWF	−0.19[a]		
	RCP2.6	−0.20	−0.23	−0.23
	RCP4.5	−0.19	−0.24	−0.25
	RCP6.0	−0.20	−0.23	−0.27
	RCP8.5	−0.20	−0.25	−0.31
NEP ($Tg\,C\,y^{-1}$)	ECMWF	−10.22		
	RCP2.6	−18.08	−33.44	−37.01
	RCP4.5	−23.03	−38.96	−45.76
	RCP6.0	−20.92	−30.27	−41.67
	RCP8.5	−18.91	−35.66	−26.95

[a] Negative values indicate methane or carbon sink.

the QTP will exert a slight warming effect on the climate system until the 2030s, but an increasingly stronger cooling effect thereafter. The tipping point was 50 years after the reference zero time point, roughly the time required for nearly complete removal of the initial CH_4 perturbation input. At the end of the 21st century, cumulative mean radiative forcing was between −0.25 and −0.35 W m^{-2}, depending on different RCP scenarios. Overall, our results show that given a sustained CH_4 source and CO_2 sink on the QTP, the net GHG warming effect will only peak after a few decades and will eventually contribute a more cooling effect to the climate system.

4. Discussion

4.1. Model optimization

Overall, our model calibration results were satisfactory, but a few tips should be mentioned when applying the global optimization method to complex system models with high parameter dimensions. Global optimization for problems without explicit analytic expressions of the objective function is challenging, because the algorithm must avoid being trapped by several local optima, while maintaining robustness in the presence of parameter interaction and non-convexity of the response surface, and having high efficiency in searching high dimensional space (Duan 2013). When applying the SCEM-UA, a trade-off between goodness of fit and computational cost is still a problem for users.

The speed of algorithm convergence highly depends on the model structure and parameter interactions. In our case, major parameters evolved to a narrow range after 100 000 total iterations (figure S2). In contrast, the MDM optimization converged much slower despite the smaller number of parameters to be optimized. We argue that this is mainly due to the multi-scalar function method used to simulate CH_4 production and oxidation. For instance, if scalars $f_1(x)$ and $f_2(x)$ are shaped with two parameters only, it is intuitive to imagine that many pairs of these two parameters can produce similar results, as long as they can adjust scalars $f_1(x)$ and $f_2(x)$ in the opposite direction. Given that the scalar approach is extensively implemented in current ecosystem models (Zhuang *et al* 2004, 2010, Wania *et al* 2013, Zhu *et al* 2014), convergence criteria (such as the Gelman and Rubin diagnostic suggested by Vrugt *et al* (2003)) can hardly be reached for most parameters when calibrating these models.

On the other hand, sub-optimal is usually sufficient in practice. Increasing the sampling size from parameter space can push the posterior of the objective function to the high-end value (figure S2), but is by no means a guarantee of better model performance. Most likely, many behavioral parameter combinations with a similar capability of reproducing the observations can be found by a search conducted in the feasible parameter space (Vrugt *et al* 2003). As shown in our example, the top 500 parameter sets (whose values can differ) for either the STM or MDM produced close goodness-of-fit and small variations in simulations (figure 2), indicating that the benefits from additional searching are marginal.

4.2. Quantification of total GHG effect

To quantify and compare the net GHG effect of a sustained CH_4 source and CO_2 sink on the QTP, the total radiative forcing rather than the more widely known metrics of the GWP was computed in our study according to Frolking *et al* (2006). As a tool originally designed for evaluating and implementing policies to control multi-GHGs, the GWP is defined as the time-integrated radiative forcing due to a pulse emission of a given component, relative to a pulse emission of an equal mass of CO_2 (IPCC, 2013). It has usually been integrated over a somewhat arbitrary time horizon of 20, 100 or 500 years, of which the choice of 100 years is most commonly adopted (e.g. CH_4 is 28 times CO_2 in terms of warming effect). Applying the GWP to biogeochemical cases could be problematic as GHG fluxes are often sustained and temporally dynamical from a long existing sink or source, even though many studies continue to use it because of its simplicity (e.g. Zhu *et al* 2013, Gatland *et al* 2014, Vanselow-Algan *et al* 2015). The method proposed by Frolking *et al* (2006) goes beyond the standard GWP approach such that (1) persistent emission or uptake of GHGs can be accounted for, and (2) the instantaneous radiative forcing for each year of simulation is quantified to allow a comparison of multiple gases in common units at any given time. Although the assumption of a near constant background atmosphere in Frolking's method is open to debate, and the decision on the appropriate pulse emission to consider (the new flux

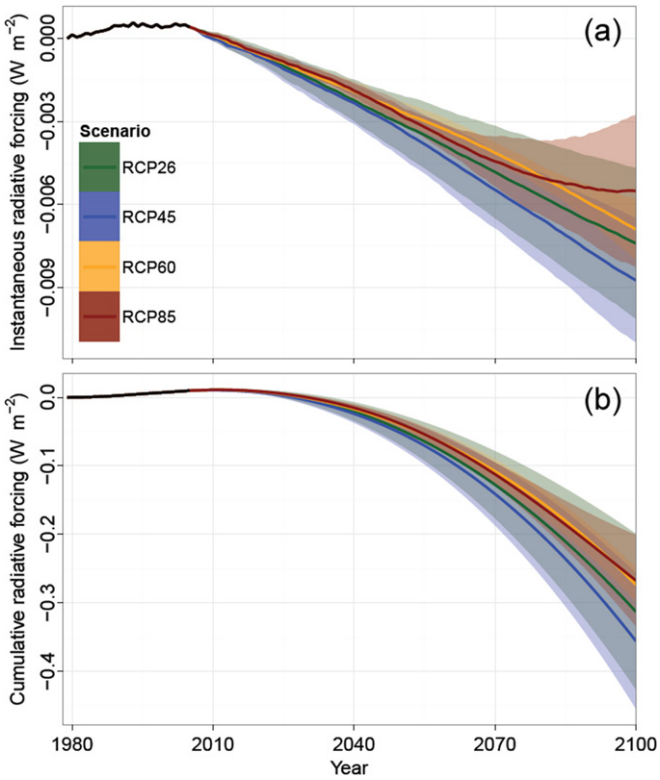

Figure 6. Instantaneous (a) and cumulative (b) radiative forcing for the period 1979–2100 calculated based on net CH_4 and CO_2 fluxes simulated with both historical (solid black line) and different RCP scenarios. Solid color lines are multi-model means, with shading representing one standard deviation.

rate versus the change in the flux rate) could greatly change the results of the simulation, it appears a useful method in biogeochemical studies when accounting for the budget of multiple sustained GHG fluxes. Frolking's method has evolved with new findings in the atmospheric sciences. For example, the fraction of CO_2 remaining in the atmosphere after a pulse input can be divided into four components (Joos *et al* 2013) instead of the original five-pool setting, and the multiplier of the indirect effect for CH_4 is now 1.65 according to IPCC (2013). A test of these and other parameter changes is beyond the scope of this study.

4.3. Uncertainties and future work

This is the first study to quantify both CH_4 emissions and net carbon exchanges on the QTP. However, the quantitative analysis is uncertain due to incomplete representation of physical and biogeochemical processes in the model (Bridgham *et al* 2013, Melton *et al* 2013, Bohn *et al* 2015), inaccurate model assumptions (Meng *et al* 2012), variations in the forcing climate data (Su *et al* 2013) and the extrapolation from site to regional scale. While progresses in model structures and mechanisms are usually slow and incremental, efforts to reducing data uncertainty are more feasible in a short period to improve model predictability.

First, seasonal and inter-annual dynamics of the wetland extent is critical to CH_4 modeling. Synthetic aperture radar (SAR) is currently the first choice to delineate wetland distribution, such as the monthly distribution of surface water extent with ~25 km sampling intervals used in this study (Papa *et al* 2010). However, optical remote sensing is highly sensitive to cloud or vegetation cover. Alternative data from passive and active microwave systems that will penetrate cloud and vegetation cover is favored (Schroeder *et al* 2010), but is currently unavailable over our study area. Some contemporary methane models, such as VIC-TEM and SDGVM, are capable of outputting dynamical wetland extent as an internal product (Hopcroft *et al* 2011, Lu and Zhuang 2012), but they tend to substantially overestimate wetland area (Melton *et al* 2013). In order to capture the seasonal flooding area, our study combined a static max potential inundation map and simulated water table depth to represent the wetland fluctuation. Improving the modeling abilities to capture wetland distribution and extent, especially the seasonality of water table dynamics, should be a research priority in the future (Zhu *et al* 2011).

The second uncertainty in quantifying CH_4 emissions on a regional scale is from the spatial-scale extrapolation across highly heterogeneous but poorly mapped wetland complexes (Bridgham *et al* 2013). In this study, we only calibrated our model at one alpine

wetland site by assuming that the remaining wetlands over the QTP have the same inert characteristics, but differ with climatic conditions. As a matter of fact, alpine wetlands on the QTP can be classified into peatlands, Marshes, and swamps, which have distinct characteristics in vegetation cover, hydrological processes, and soil history (Chen *et al* 2013). However, due to severe field experimental conditions, high quality observational data are mostly limited to the Lunhaizi wetland in Haibei Station (Hirota *et al* 2004, Yu *et al* 2013) and the Zoige wetland (Chen et al 2009, 2013). Field researchers should consider expanding field measurement footprints in the future, and data sharing with modelers is highly recommended.

Finally, much of the uncertainty in future projections is due to the poor agreement among CMIP5 GCMs under the RCP scenarios (figures S3, S4). The majority of the GCMs have cold biases of 1.1–2.5 °C in air temperature for the QTP, while they overestimate annual mean precipitation by 62%–183% (Su *et al* 2013). A multi-model ensemble approach, as was suggested in the IPCC AR5 report (IPCC, 2013), was used to configure the climatology uncertainty. While the statistical interpolation method used to generate fine resolution data is simple and computationally efficient (Wilby *et al* 1998), dynamical downscaling with regional climate models was more ideal to compensate for the shortage of coarse output from GCMs and to capture details of the complex surface properties of the QTP (Ji and Kang 2012). However, due to the high computational cost, dynamically downscaling climate data that cover representative GCMs under all RCP scenarios is generally not available to ecosystem modelers. A publicly accessible database like this would greatly benefit the research community in future studies.

5. Conclusions

Using a coupled biogeochemistry model framework, this study analyzed the carbon-based GHG dynamics over the QTP for the period 1979–2100. Our model simulations at the site level were able to closely match the field-observed soil temperature and CH_4 flux after calibrating the model parameters using the SCEM-UA global optimization algorithm. Our study showed that the region currently acts as a CH_4 source (emissions of 0.95 Tg CH_4 y^{-1} and consumption of 0.19 Tg CH_4 y^{-1}) and a CO_2 sink (14.1 Tg C y^{-1}). In response to future climate change, the CH_4 source and the CO_2 sink strengthened, leading to an increasingly negative perturbation of radiative forcing. The spatial patterns and temporal trends of the NME and NEP highly depend on the RCP scenario. Climate-induced changes in the magnitude of the NME were statistically significant for most of the QTP, while spatial changes in the NEP were only significantly apparent under RCP4.5 and RCP6.0. The instantaneous radiative forcing impact is determined by persistent CO_2 sequestration and recent (~5 decades) CH_4 emission. The cumulative GHG effect was a negative feedback (cooling) to the climate system at the end of the 21st century. Uncertainties in our model estimations can be reduced by including more explicit information on wetland distribution and classification, and more reliable future climate scenarios. Additional observational data from representative wetland ecosystems shall be collected to improve future quantification of these carbon-based GHGs.

Acknowledgments

This research is partially supported by funding to Q Z through an NSF project (DEB- #0919331), the NASA Land Use and Land Cover Change program (NASA-NNX09AI26G), the Department of Energy (DE-FG02-08ER64599), and the NSF Division of Information & Intelligent Systems (NSF-1028291). Jin-Sheng He and Weiming Song are supported by the National Basic Research Program of China (grant number 2014CB954004) and the National Natural Science Foundation of China (grant numbers 31270481 and 31025005).

References

Bohn T J *et al* 2015 WETCHIMP-WSL: intercomparison of wetland methane emissions models over West Siberia *Biogeosciences* **12** 1907–73

Bridgham S D, Cadillo-Quiroz H, Keller J K and Zhuang Q 2013 Methane emissions from wetlands: biogeochemical, microbial, and modeling perspectives from local to global scales *Global change biol.* **19** 1325–46

Cao G, Xu X, Long R, Wang Q, Wang C, Du Y and Zhao X 2008 Methane emissions by alpine plant communities in the Qinghai–Tibet Plateau *Biol. Lett.* **4** 681–4

Chen H, Wu N, Gao Y, Wang Y, Luo P and Tian J 2009 Spatial variations on methane emissions from Zoige alpine wetlands of Southwest China *Sci. Total Environ.* **407** 1097–104

Chen H, Wu N, Yao S, Gao Y, Wang Y, Tian J and Yuan X 2010 Diurnal variation of methane emissions from an alpine wetland on the eastern edge of Qinghai-Tibetan Plateau *Environ. Monit. Assess.* **164** 21–8

Chen H, Zhu Q a, Peng C, Wu N, Wang Y, Fang X, Jiang H, Xiang W, Chang J and Deng X 2013 Methane emissions from rice paddies natural wetlands, lakes in China: synthesis new estimate *Global change biol.* **19** 19–32

Dee D, Uppala S, Simmons A, Berrisford P, Poli P, Kobayashi S, Andrae U, Balmaseda M, Balsamo G and Bauer P 2011 The ERA-Interim reanalysis: configuration and performance of the data assimilation system *Q. J. R. Meteorol. Soc.* **137** 553–97

Ding W, Cai Z and Wang D 2004 Preliminary budget of methane emissions from natural wetlands in China *Atmos. Environ.* **38** 751–9

Ding W-X and Cai Z-C 2007 Methane emission from natural wetlands in China: summary of years 1995–2004 studies *Pedosphere* **17** 475–86

Duan Q 2003 Global optimization for watershed model calibration *Calibration of Watershed Models* (Washington, DC: American Geophysical Union) pp 89–104

Fang J, Yang Y, Ma W, Mohammat A and Shen H 2010 Ecosystem carbon stocks and their changes in China's grasslands *Sci. China Life Sci* **53** 757–65

Frauenfeld O W, Zhang T and Serreze M C 2005 Climate change and variability using European Centre for Medium-Range Weather Forecasts reanalysis (ERA-40) temperatures on the Tibetan Plateau *J. Geophys. Res.: Atmos.* **110** D02101

Frolking S, Roulet N and Fuglestvedt J 2006 How northern peatlands influence the Earth's radiative budget: sustained methane emission versus sustained carbon sequestration *J. Geophys. Res.: Biogeosci.* **111** G01008

Gabriel E *et al* 2004 Open MPI: goals, concept, and design of a next generation MPI implementation *Recent Advances in Parallel Virtual Machine and Message Passing Interface* (Berlin: Springer) pp 97–104

Gatland J R, Santos I R, Maher D T, Duncan T M and Erler D V 2014 Carbon dioxide and methane emissions from an artificially drained coastal wetland during a flood: Implications for wetland global warming *J. Geophys. Res.: Biogeosci.* **198** 1698–1716

Hirota M, Tang Y, Hu Q, Hirata S, Kato T, Mo W, Cao G and Mariko S 2004 Methane emissions from different vegetation zones in a Qinghai-Tibetan Plateau wetland *Soil Biol. Biochem.* **36** 737–48

Hopcroft P O, Valdes P J and Beerling D J 2011 Simulating idealized Dansgaard-Oeschger events and their potential impacts on the global methane cycle *Quat. Sci. Rev.* **30** 3258–68

IPCC 2013 *Climate Change 2013: The Physical Science Basis. Contribution of Working Group I to the Fifth Assessment Report of the Intergovernmental Panel on Climate Change* ed T F Stocker *et al* (Cambridge, United Kingdom: Cambridge University Press) p 1535

Ji Z and Kang S 2012 Double-nested dynamical downscaling experiments over the Tibetan Plateau and their projection of climate change under two RCP scenarios *J. Atmos. Sci.* **70** 1278–90

Jin H, Cheng G, Xu B and Nakano T 1998 Study on CH4 fluxes from alpine wetlands at the Huashixia Permafrost Station, Tibetan Plateau *J. Glaciol. Geol.* **20** 167–9

Jin H, Wu J, Cheng G, Nakano T and Sun G 1999 Methane emissions from wetlands on the Qinghai-Tibet Plateau *Chin. Sci. Bull.* **44** 2282–6

Jin Z, Zhuang Q, He J-S, Luo T and Shi Y 2013 Phenology shift from 1989 to 2008 on the Tibetan Plateau: an analysis with a process-based soil physical model and remote sensing data *Clim. change* **119** 435–49

Jin Z, Zhuang Q, Dukes J S, He J-S, Chen M, Zhang T, Sokolov A and Luo T 2015 An ecosystem modeling analysis of phenology acclimation and carbon cycling on the Tibetan Plateau during the 21st century, submitted

Joos F *et al* 2013 Carbon dioxide and climate impulse response functions for the computation of greenhouse gas metrics: a multi-model analysis *Atmos. Chem. Phys.* **13** 2793–825

Kato T, Hirota M, Tang Y and Wada E 2011 Spatial variability of CH_4 and N_2 O fluxes in alpine ecosystems on the Qinghai–Tibetan Plateau *Atmos. Environ.* **45** 5632–9

Kato T, Yamada K, Tang Y, Yoshida N and Wada E 2013 Stable carbon isotopic evidence of methane consumption and production in three alpine ecosystems on the Qinghai–Tibetan Plateau *Atmos. Environ.* **77** 338–47

Kirschke S, Bousquet P, Ciais P, Saunois M, Canadell J G, Dlugokencky E J, Bergamaschi P, Bergmann D, Blake D R and Bruhwiler L 2013 Three decades of global methane sources and sinks *Nat. Geosci.* **6** 813–23

Loveland T R, Reed B C, Brown J F, Ohlen D O, Zhu Z, Yang L and Merchant J W 2000 Development of a global land cover characteristics database and IGBP DISCover from 1 km AVHRR data *Int. J. Remote Sens.* **21** 1303–30

Lu X and Zhuang Q 2012 Modeling methane emissions from the Alaskan Yukon River basin, 1986–2005, by coupling a large-scale hydrological model and a process-based methane model *J. Geophys. Res.: Biogeosci.* **117** G02010

Melton J, Wania R, Hodson E, Poulter B, Ringeval B, Spahni R, Bohn T, Avis C, Beerling D and Chen G 2013 Present state of global wetland extent and wetland methane modelling: conclusions from a model inter-comparison project (WETCHIMP) *Biogeosci.* **10** 753–88

Meng L, Hess P, Mahowald N, Yavitt J, Riley W, Subin Z, Lawrence D, Swenson S, Jauhiainen J and Fuka D 2012 Sensitivity of wetland methane emissions to model assumptions: application and model testing against site observations *Biogeosci.* **9** 2793–819

Niu Z, Zhang H, Wang X, Yao W, Zhou D, Zhao K, Zhao H, Li N, Huang H and Li C 2012 Mapping wetland changes in China between 1978 and 2008 *Chin. Sci. Bull.* **57** 2813–23

Olefeldt D, Turetsky M R, Crill P M and McGuire A D 2013 Environmental and physical controls on northern terrestrial methane emissions across permafrost zones *Global change biol.* **19** 589–603

Papa F, Prigent C, Aires F, Jimenez C, Rossow W and Matthews E 2010 Interannual variability of surface water extent at the global scale, 1993–2004 *J. Geophys. Res.: Atmos.* **115** D12111

Piao S, Tan K, Nan H, Ciais P, Fang J, Wang T, Vuichard N and Zhu B 2012 Impacts of climate and CO_2 changes on the vegetation growth and carbon balance of Qinghai–Tibetan grasslands over the past five decades Glob *Planet. Change* **98** 73–80

Schroeder R, Rawlins M, McDonald K, Podest E, Zimmermann R and Kueppers M 2010 Satellite microwave remote sensing of North Eurasian inundation dynamics: development of coarse-resolution products and comparison with high-resolution synthetic aperture radar data *Environ. Res. Lett.* **5** 015003

Shindell D T, Faluvegi G, Koch D M, Schmidt G A, Unger N and Bauer S E 2009 Improved attribution of climate forcing to emissions *Science* **326** 716–8

Song W, Wang G, Wang H, Chen L, Jin Z, Zhuang Q and He J-S 2015 Methane emissions from an alpine wetland on the Tibetan Plateau: neglected but vital contribution of non-growing season *J. Geophys. Res.: Biogeosci.* at press

Spahni R, Wania R, Neef L, Weele M v, Pison I, Bousquet P, Frankenberg C, Foster P, Joos F and Prentice I 2011 Constraining global methane emissions and uptake by ecosystems *Biogeosci.* **8** 1643–65

Su F, Duan X, Chen D, Hao Z and Cuo L 2013 Evaluation of the global climate models in the CMIP5 over the Tibetan Plateau *J. Clim.* **26** 3187–208

Vanselow-Algan M, Schmidt S R, Greven M, Fiencke C, Kutzbach L and Pfeiffer E M 2015 High methane emissions dominate annual greenhouse gas balances 30 years after bog rewetting *Biogeosci. Discuss.* **12** 2809–42

Vörösmarty C J, Moore B, Grace A L, Gildea M P, Melillo J M, Peterson B J, Rastetter E B and Steudler P A 1989 Continental scale models of water balance and fluvial transport: an application to South America *Glob. Biogeochem. Cycles* **3** 241–65

Vrugt J A, Gupta H V, Bouten W and Sorooshian S 2003 A shuffled complex evolution metropolis algorithm for optimization and uncertainty assessment of hydrologic model parameters *Water Resour. Res.* **39** 1201

Vrugt J A, Nualláin B Ó, Robinson B A, Bouten W, Dekker S C and Sloot P M 2006 Application of parallel computing to stochastic parameter estimation in environmental models *Comput. Geosci.* **32** 1139–55

Wania R, Melton J, Hodson E, Poulter B, Ringeval B, Spahni R, Bohn T, Avis C, Chen G and Eliseev A 2013 Present state of global wetland extent and wetland methane modelling: methodology of a model inter-comparison project (WETCHIMP) *Geosci. Model Dev.* **6** 617–41

Wania R, Ross I and Prentice I C 2009 Integrating peatlands and permafrost into a dynamic global vegetation model: 1. Evaluation and sensitivity of physical land surface processes *Glob. Biogeochem. Cycles* **23** GB3014

Wei D, Wang Y, Wang Y, Liu Y and Yao T 2012 Responses of CO_2, CH_4 and $N2_O$ fluxes to livestock exclosure in an alpine steppe on the Tibetan Plateau, China *Plant and Soil* **359** 45–55

Wei S, Dai Y, Liu B, Zhu A, Duan Q, Wu L, Ji D, Ye A, Yuan H and Zhang Q 2013 A China data set of soil properties for land surface modeling *J. Adv. Model. Earth Syst.* **5** 212–24

Wilby R L, Wigley T M L, Conway D, Jones P D, Hewitson B C, Main J and Wilks D S 1998 Statistical downscaling of general circulation model output: a comparison of methods *Water Resour. Res.* **34** 2995–3008

Xu K, Kong C, Liu J and Wu Y 2010 Using methane dynamic model to estimate methane emission from natural wetlands in China, *Geoinformatics, 2010 18th Int. Conf. on: IEEE* pp 1–4

Yi S, Wang X, Qin Y, Xiang B and Ding Y 2014 Responses of alpine grassland on Qinghai–Tibetan plateau to climate warming and permafrost degradation: a modeling perspective *Environ. Res. Lett.* **9** 074014

Yu H 2002 Rmpi: parallel statistical computing in R *R News* **2** 10–4

Yu L, Wang H, Wang G, Song W, Huang Y, Li S-G, Liang N, Tang Y and He J-S 2013 A comparison of methane emission measurements using eddy covariance and manual and automated chamber-based techniques in Tibetan Plateau alpine wetland *Environ. Pollut.* **181** 81–90

Zhang X and Jiang H 2014 Spatial variations in methane emissions from natural wetlands in China *Int. J. Environ. Sci. Technol.* **11** 77–86

Zhu Q, Liu J, Peng C, Chen H, Fang X, Jiang H, Yang G, Zhu D, Wang W and Zhou X 2014 Modelling methane emissions from natural wetlands by development and application of the TRIPLEX-GHG model *Geosci. Model Dev.* **7** 981–99

Zhu X, Zhuang Q, Chen M, Sirin A, Melillo J, Kicklighter D, Sokolov A and Song L 2011 Rising methane emissions in response to climate change in Northern Eurasia during the 21st century *Environ. Res. Lett.* **6** 045211

Zhu X, Zhuang Q, Gao X, Sokolov A and Schlosser C A 2013 Pan-Arctic land–atmospheric fluxes of methane and carbon dioxide in response to climate change over the 21st century *Environ. Res. Lett.* **8** 045003

Zhuang Q, Chen M, Xu K, Tang J, Saikawa E, Lu Y, Melillo J M, Prinn R G and McGuire A D 2013 Response of global soil consumption of atmospheric methane to changes in atmospheric climate and nitrogen deposition *Glob. Biogeochem. Cycles* **27** 650–63

Zhuang Q, He J, Lu Y, Ji L, Xiao J and Luo T 2010 Carbon dynamics of terrestrial ecosystems on the Tibetan Plateau during the 20th century: an analysis with a process-based biogeochemical model *Glob. Ecol. Biogeogr.* **19** 649–62

Zhuang Q, Melillo J M, Kicklighter D W, Prinn R G, McGuire A D, Steudler P A, Felzer B S and Hu S 2004 Methane fluxes between terrestrial ecosystems and the atmosphere at northern high latitudes during the past century: a retrospective analysis with a process-based biogeochemistry model *Glob. Biogeochem. Cycles* **18** GB3010